Interaction between *Neisseria gonorrhoeae* bacterial peroxidase and its electron donor, the lipid-modified azurin

Cláudia S. Nóbrega and Sofia R. Pauleta [iD]

Microbial Stress Lab, UCIBIO, REQUIMTE, Department of Química, Faculdade de Ciências e Tecnologia, Universidade Nova de Lisboa, Caparica, Portugal

Correspondence

S. R. Pauleta, Microbial Stress Lab, UCIBIO, REQUIMTE, Department of Química, Faculdade de Ciências e Tecnologia, Universidade Nova de Lisboa, Caparica, 2829-516, Portugal
Fax: + 351 351 212 948 550
Tel: +351 212948385, ext 10967
E-mail: srp@fct.unl.pt

The *Neisseria gonorrhoeae* bacterial cytochrome *c* peroxidase plays a key role in detoxifying the cells from H_2O_2 by reducing it to water using the lipid-modified azurin, LAz, a small type 1 copper protein, as electron donor. Here, the interaction between these two proteins was characterized by steady-state kinetics, two-dimensional NMR and molecular docking simulations. LAz is an efficient electron donor capable of activating this enzyme. This electron transfer complex is weak with a hydrophobic character, with LAz binding close to the electron transferring heme of the enzyme. The high catalytic rate (39 ± 0.03 s^{-1}) is explained by the LAz pre-orientation, due to a positive dipole moment, and by the fast-dynamic ensemble of orientations, suggested by the small chemical shifts.

Pathogenic bacteria, such as *Neisseria gonorrhoeae* that causes the sexually transmitted disease gonorrhea, are constantly exposed to reactive oxygen species (ROS) and have developed numerous defense mechanisms to cope with oxidative stress [1]. Bacterial cytochrome *c* peroxidase (BCCP) is one of the enzymes involved in ROS detoxification. This enzyme catalyzes the reduction in hydrogen peroxide to water [2], with the required electrons being donated by small electron shuttle proteins, of the respiratory chain, such as small *c*-type cytochromes [3–5] or type 1 copper proteins [6–10].

In *N. gonorrhoeae*, a mutant strain lacking the gene coding for a cupredoxin, the lipid-modified azurin (LAz), was more sensitive to hydrogen peroxide but not to superoxide, resulting in reduced survival in human ectocervical epithelial cells [11]. Therefore, LAz

was proposed to be the physiological electron donor of BCCP (*Ng*BCCP) [12], donating electrons to the high potential electron transferring heme (E heme), which are then transferred to the low potential peroxidatic heme (P heme), where catalysis occurs [13]. This small type 1 copper protein has a high sequence homology to other copper proteins from the azurin family [14,15] and it has an unique additional N-terminal region of 39 amino acids that encodes the H.8 epitope (common in *Neisseria* genus), in which there are five imperfect repeats of a sequence rich in alanines (AAEAP) [14,16]. Thus, like *Ng*BCCP [17], LAz is a lipid-modified protein, bound to the outer membrane [16] by a palmityl fatty acid at the N-terminus [11,14,18].

The solution structure of holo-LAz is an elongated β-barrel formed by eight β-strands that form two

Abbreviations

APBS, Adaptive Poisson-Boltzmann Solver; BCCP, bacterial cytochrome *c* peroxidase; DAD, diaminodurol; E heme, electron transferring heme; ET, electron transfer; LAz, lipid-modified azurin; NgBCCP, Neisseria gonorrhoeae BCCP; P heme, peroxidatic heme; ROS, reactive oxygen species; $\Delta^i G$, free energy gain.

antiparallel β-sheets, arranged in the Greek key motif with one main alpha helix after β4 [12]. LAz belongs to the azurin family given its copper center (coordinated by the side chains of His49, Cys113, His118, Met122 and the oxygen of the peptide bond from Gly48), together with its topology and spectroscopic properties [12].

Azurins have unique spectroscopic properties, as well as the ability to transfer electrons rapidly to several enzymes [19,20]. Electron transfer (ET) requires specificity but, it must also be fast enough to support the rapid turnover rates needed to complete a catalytic cycle. In these transient complexes, partners are proposed to pre-orient due to large dipole moments, as observed for two redox shuttles from *Paracoccus pantotrophus*, pseudoazurin and cytochrome c_{550} [6,7]. In these, the dipole vector exits the protein surface at the point proposed to be involved in ET, that is, at the solvent-exposed copper center ligand in cupredoxins or at the solvent-exposed heme edge in cytochromes [7]. After collision of the ET complex partners, a range of small conformational changes allows lateral fluidity on each other surface to find the productive ET positions. The association between the two proteins must be weak, to favor rapid dissociation, the reason why these proteins have very small structural changes between their oxidized and reduced forms [2,21].

This work focusses on the physiological ET complex between the soluble globular domains of *Ng*BCCP and LAz. This interaction will be addressed by steady-state kinetics, NMR and molecular docking simulations, revealing its weak transient nature and an ET pathway is proposed for a top model complex.

Materials and methods

Protein sample preparation

The two proteins were heterologously produced in *Escherichia coli* BL21 (DE3) and purified, in a soluble form without the N-terminal H.8 epitope region as previously described [13,22]. Proteins' concentration was determined using the extinction coefficient established before [12,13].

*Ng*BCCP kinetics assays with LAz

The assay was performed at 25 °C in the same buffer, containing 10 μM reduced LAz, 100 μM H_2O_2 (for the Michaelis–Menten curve H_2O_2 ranged between 0.01 and 1 mM), and initiated with 10 nM pre-activated *Ng*BCCP [13]. At the end of the assay, a small aliquot of potassium ferricyanide concentrated solution was added to fully

oxidize LAz and confirm that all electron donor was oxidized.

The temperature and pH dependence of the peroxidase activity were assessed between 15 and 60 ° and by varying the buffer pH at a concentration of 10 mM, (MES buffer with pH: 5.5–6.5; HEPES buffer with pH: 6.5–8.0; Bis-Tris Propane buffer with pH: 8.0–9.5). pH values below 5.5 were not tested as LAz is not stable. The ionic strength dependence was studied by adding NaCl to the assay buffer at different concentrations (0–500 mM).

In the *Ng*BCCP activation assay by LAz, 10 nM of as-isolated *Ng*BCCP were incubated with 9 μM reduced LAz in 10 mM MES, pH 6.0, 10 mM NaCl, and 1 mM $CaCl_2$ for different times. The kinetic assay was initiated by adding 100 μM H_2O_2.

The observed initial rates, v_{obs}, were determined in the first seconds of the re-oxidation curve. The turnover number was normalized by the electron donor concentration (k_{cat}/[LAz]) for comparison. The pH dependence of the kinetic data was simulated using a bell-shaped function, Eqn (1) [23]:

$$v = \frac{v_{max}}{1 + 10^{(pKa_1 - pH)} + 10^{(pH - pKa_2)}} \tag{1}$$

in which the reaction rate, v, is given as a function of pH considering two pKa values.

Two-dimensional NMR titration

Two-dimensional heteronuclear NMR spectra were recorded for a 0.1 mM ^{15}N labeled LAz solution in 5 mM HEPES pH 7.0, 2 mM $CaCl_2$, 10% D_2O, 1 mM sodium ascorbate and 1 μM diaminodurol (DAD). NMR spectra were recorded for a 1 : 0, 1 : 1 and 1 : 2 LAz : *Ng*BCCP ratio. Both the *Ng*BCCP E heme (*Ng*BCCP in the mixed-valence state) and LAz were reduced with 1 mM sodium ascorbate. All NMR tubes were kept under an argon stream for a few minutes and then sealed to guarantee that the concentration of oxygen was low, and no re-oxidation occurred during the experiments.

The spectra were acquired in a Bruker Avance III 600 MHz equipped with a TCI-cryoprobe at 298 K. Each spectrum had a total of 16 scans. The spectral widths were 9600 Hz for ^1H (16 p.p.m.; 1024 transients) and 2400 Hz for ^{15}N (40 p.p.m.; 128 transients). NMR spectra were processed with TOPSPIN 3.5 (Bruker Corporation, Billerica, MA, USA) provided by Bruker and analyzed in CARA 1.9.0 (Kurt Wüthrich at the Swiss Federal Institute of Technology ETH, Zurich, Switzerland). LAz assignment deposited under the accession number 18636 in BMRB [22] was used for data analysis. Chemical shifts of each resonance $\Delta\delta_{HN}$ (p.p.m.), were calculated considering the changes in the proton $\Delta\delta_H$ (p.p.m.) and nitrogen $\Delta\delta_N$ (p.p.m.) according to Eqn (2) [24]:

$$\Delta\delta_{HN} = \frac{\sqrt{\Delta\delta_H^2 + \frac{\Delta\delta_N^2}{25}}}{2} \tag{2}$$

Dipole moment calculations

The dipole moment was determined in CHIMERA 1.10.2 for each protein structure [25]. The hydrogen atoms were added, and charges were attributed to each protein structure using Amber. The charge of the copper atom was assigned to +1 or +2 for the reduced or oxidized protein, respectively. The dipole vector was determined in Chimera using the 'dipole.py' python script (http://plato.cgl.ucsf.edu/trac/chimera/wiki/Scripts).

Bioinformatic analysis

The protein electrostatic surface was analyzed using Adaptive Poisson-Boltzmann Solver (APBS [26,27]). The PDB files were treated in PDB2PQR [28] (http://nbcr-222.ucsd.edu/pdb2pqr_2.1.1/). The final PQR file from PDB2PQR was used as input in the APBS (http://www.poissonboltzmann.org/) to determine electrostatic properties using default parameters. The solvent accessible surface was colored according to electrostatic potential in Chimera, from −5 to +5 kT/e (red to blue). The hydrophobic surface was rendered in BIOVIA DISCOVERY STUDIO VISUALIZER 4.5 (Dassault Systémes BIOVIA, San Diego, CA, USA), colored from non-hydrophobic residues, in green, to hydrophobic residues, in magenta (−3 to +3: color scale green-white-magenta).

Molecular docking simulation

The docking algorithms used in this work were BiGGER [29] and ZDOCK [30,31]. The dimer of *Ng*BCCP in the mixed-valence state (model structure [13]) was considered the target and the first model of the LAz NMR structure (PDB ID: 2N0M) the probe. BiGGER was implemented in CHIMERA 3.07 (Ludwig Krippahl and Nuno Palma, FCT-UNL, Caparica, Portugal). A 'soft dock' was performed with a complete and systematic search in space by rotating LAz around the surface of *Ng*BCCP with a translation and rotation steps of 1 Å resolution and 15°. A maximum of 5000 solutions were selected with 150 minimum contacts. The top six cluster conformations with highest global and hydrophobic score were analyzed. ZDOCK docking was performed in the ZDOCK web-based server 3.0.2 (http://zdock.umassmed.edu/). The output consists of 2000 models with a combined score based on electrostatics, shape complementarity, and statistical potential terms. The five top models were analyzed.

The geometrical and physicochemical properties of each top complex were determined according to Jones and Thornton [32] using PDBePISA [33] and ProFACE [34] for the protein–protein interface analysis. The ET pathway was analyzed in PATHWAYS [35,36].

Results and Discussion

*Ng*BCCP steady-state kinetics using LAz as electron donor

Previously, it was shown that *Ng*BCCP has peroxidase activity using a synthetic electron donor, $ABTS^{2-}$ [13] as electron source, and that it needs reductive activation in the presence of calcium ions to reach maximum activity. Here, it was evaluated whether LAz was able to activate *Ng*BCCP and how fast this process is. Without pre-incubation with LAz (0 min), *Ng*BCCP has approximately half-maximum activity and after 10 min of incubation, it attains maximum activity (Fig. S1). These results indicate that LAz donates electrons to E heme, activating *Ng*BCCP, and maintaining its catalytic activity. This can be attributed to a specific interaction between the two proteins and also to the reduction potential of LAz (277 ± 5 mV, at pH 7.0 [12]) that is close to the one of *Ng*BCCP E heme (+310 ± 10 mV, at pH 7.5 [13]).

The kinetic assays were performed in the presence or absence of calcium ions and the initial oxidation rates were 0.329 ± 0.004 μM LAz·s^{-1} and 0.085 ± 0.003 μM LAz·s^{-1}, respectively (Fig. S2). Therefore, calcium ions are needed for maximum activity, as previously shown for the *Ng*BCCP/$ABTS^{2-}$ pair. This could also be an indication that formation of a productive ET complex is dependent on calcium ions, probably due to a simplification of the *Ng*BCCP solution states [13].

The kinetic parameters for the pre-activated *Ng*BCCP catalytic activity with LAz as electron donor were a K_M of 0.4 ± 0.2 μM H_2O_2 and a turnover number of 39 ± 0.03 s^{-1}, at pH 6.0 and at 25 °C, by fitting the data to the Michaelis–Menten equation (Fig. 1A). Compared to $ABTS^{2-}$ as electron donor [13], the K_M decreased about one order of magnitude (from 4 to 0.4 μM H_2O_2), which shows the high affinity of *Ng*BCCP for hydrogen peroxide. The turnover number is lower because LAz is not used in the assay at saturating concentrations, as occurred with $ABTS^{2-}$.

Analysis of these kinetic parameters suggests that the LAz/*Ng*BCCP pair is more efficient than the $ABTS^{2-}$/*Ng*BCCP pair, since the turnover number is high (39 s^{-1} compared to 79 s^{-1}, for LAz/*Ng*BCCP and $ABTS^{2-}$/*Ng*BCCP respectively), even using nonsaturating LAz concentrations. In addition, in the LAz/*Ng*BCCP pair ET is dependent on-site recognition, in contrast to $ABTS^{2-}$, a small molecule used at saturating conditions that might be able to donate electrons directly to P heme.

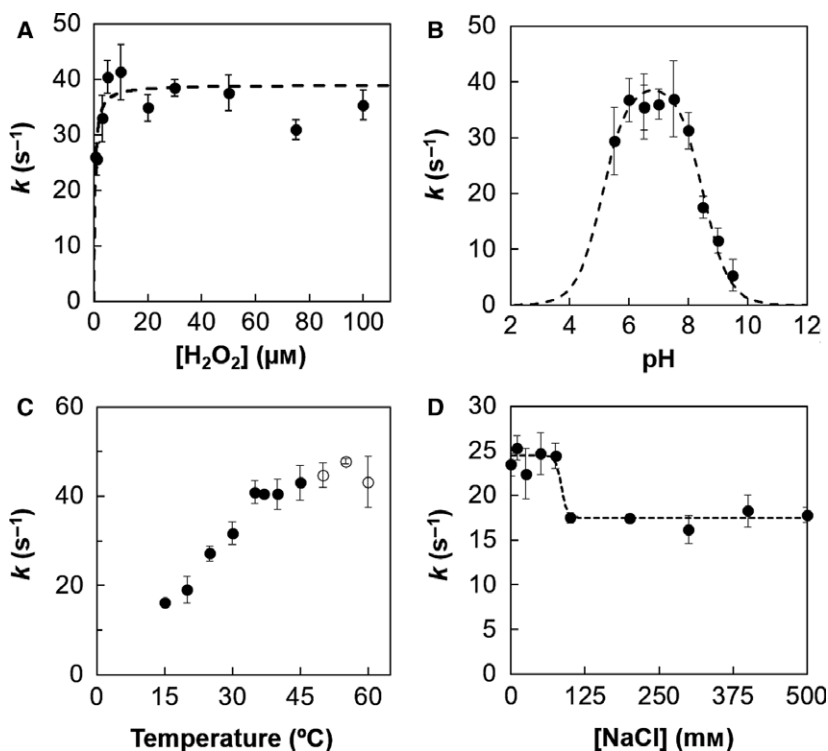To compare the kinetic parameters of *Ng*BCCP with other BCCPs, the turnover number was corrected for

Fig. 1. Steady-state kinetics using LAz as electron donor. Catalytic activity of pre-activated NgBCCP as a function of substrate concentration (A), pH (B), temperature (C), and ionic strengh (D). The open circles in (C) are experimental points where the reaction is not complete due to NgBCCP denaturation. The dashed lines represent the simulated data using the Michaelis Menten equation and the bell-shaped Eqn (1).

the electron donor concentration, $k_{cat}/[ED]$. This comparison is valid since the amount of electron donor in the assays is typically much lower than the expected electron donor K_M value (60 μM cytochrome c_2 from *Rhodobacter capsulatus* [37] and ~ 70 μM pseudoazurin from *P. pantotrophus* [7]). At 25 °C, pH 6.0, the $k_{cat}/[LAz] = 3.9$ μM^{-1}·s^{-1}, which is in the same order of magnitude as the one determined for BCCP/cytochrome c_2 in *R. capsulatus* (2 μM^{-1}·s^{-1}) [37].

Regarding the pH dependence (Fig. 1B), the catalytic activity was simulated with a bell-shaped curve with an optimum pH at 6.8, and with a $pKa_1 = 5.1 \pm 0.1$ and a $pKa_2 = 8.5 \pm 0.1$, similar to that observed with ABTS^{2-} (5.9 ± 0.1 and 8.4 ± 0.1, respectively) [13]. Compared to the ABTS^{2-} assay, the apparent pKa_1, when LAz is used as electron donor, is lower, because ABTS^{2-} is unable to sustain enzyme activity below pH 6.0, while LAz is (confirmed by its complete oxidation by NgBCCP at the end of the assay in this pH range). Therefore, as the pKa values reported for LAz/NgBCCP and ABTS^{2-}/NgBCCP pairs are similar, they might reflect changes on the protonation/deprotonation of key residues in the peroxidase, rather than in the ET complex.

The peroxidase activity increases with temperature, up to 37 °C, the human body temperature (similar rates from 35 to 45 °C), and afterward it apparently increases but the assays are incomplete, as LAz is not completely

oxidized by NgBCCP (Fig. 1C). This is attributed to NgBCCP inactivation at temperatures > 50 °C, as the mixed-valence NgBCCP has a T_m of 55.6 °C [13]. Although LAz T_m was not determined, the copper atom is not lost at the end of the assay (estimated from A$_{625\ nm}$), which indicates that LAz is not denatured.

At ionic strength values higher than 100 mM, LAz oxidation rates decrease 29%, while above and below this value, there is a plateau with no significant change in activity (Fig. 1D). This is an indication that LAz/NgBCCP interaction has a hydrophobic nature [38]. Moreover, the small decrease in catalytic activity between 80 and 100 mM NaCl can be explained by formation of a more productive complex at lower ionic strength, possibly due to changes in the proteins solvation shell. Transient interfaces tend to be rich in water molecules ('wet') [21,39] and although hydrophobic interfaces are characterized by a more complete desolvation, in some cases the water molecules at the interface form water-mediated polar interactions that contribute to the stability of the ET complex [39].

Heteronuclear NMR titration and surface analysis

The assigned ^{1}H–^{15}N HSQC spectra of reduced LAz was used to identify LAz residues that are affected by the binding of NgBCCP [22]. For that, the ^{1}H–^{15}N HSQC spectra of three independent ascorbate-reduced
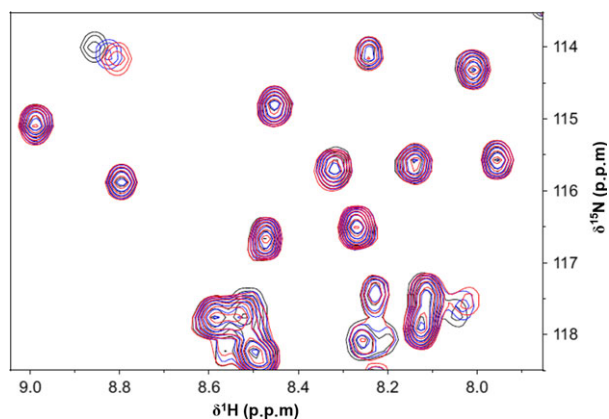
Fig. 2. Overlay of the spectral region of the ^1H–^{15}N HSQC spectra of free LAz (black) and after addition of one (blue) or two (red) equivalents of NgBCCP. The ^NH resonance of three of the residues that experience the higher chemical shifts are present in this region.

samples were acquired at LAz : *Ng*BCCP ratios of 1 : 0, 1 : 1 and 1 : 2 (Fig. 2). His85 and Lys87 experienced the highest chemical shifts (0.060 and 0.056 p.p.m., respectively) and the amide region of these residues is shown in the overlaid ^1H–^{15}N HSQC spectra

of the three samples (Fig. 2), indicating that the binding occurs in a fast exchange regime in the NMR timescale.

The combined proton and nitrogen chemical shifts variation in LAz amide resonances upon *Ng*BCCP binding in a 1 : 1 and 1 : 2 ratio was analyzed using Eqn (2) (Fig. 3A,B). The increase in chemical shifts variation, from a 1 : 1 to a 1 : 2 ratio, is explained considering that the binding is weak and that in a 1 : 1 ratio, not all LAz molecules are bound to *Ng*BCCP. The affected residues were divided into three groups: $\Delta\delta_{HN} \geq 0.025$ p.p.m., in red; $\Delta\delta_{HN}$ between 0.015–0.025 p.p.m. in blue; $\Delta\delta_{HN}$ between 0.005 and 0.015 p.p.m. in grey; and mapped onto the surface of LAz (Fig. 3C). The main affected region in LAz surface comprises the residues 74–87, which is a loop region (mapped in Fig. 3C; $\Delta\delta_{HN} \geq 0.025$ p.p.m.: Tyr74, Val75, Val82, His85 and Lys87 in red; $0.015 > \Delta\delta_{HN} > 0.025$ p.p.m.: Asp78, Asp79, Ala80, Ala84, and Thr86 in blue). Gly58, Cys113 and His118 that coordinate the copper center are included in the group with the lowest chemical shift ($0.005 > \Delta\delta_{HN} > 0.015$ p.p.m., in grey). A closer look at LAz solution structure shows that this loop in solution is slightly aside from the β-barrel, forming a small
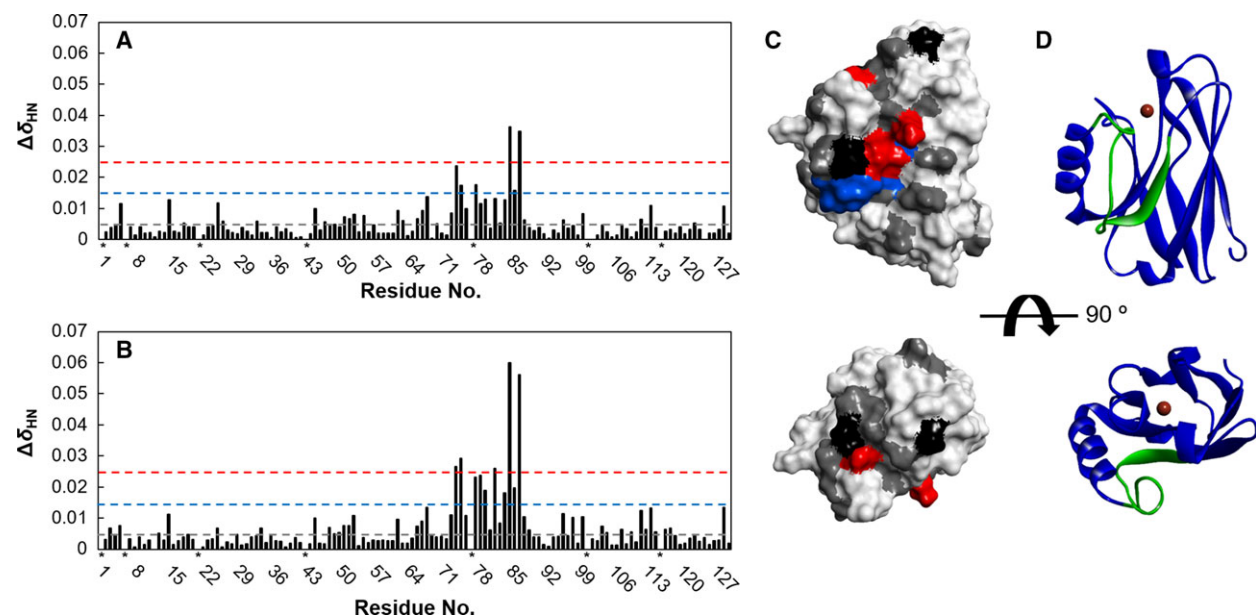

Fig. 3. Chemical shift variation in LAz resonances upon *Ng*BCCP binding in a 1 : 1 (A) and 1 : 2 (B) ratio. The chemical shifts were categorized into three groups: $\Delta\delta_{HN} \geq 0.025$ p.p.m., $0.015 < \Delta\delta_{HN} < 0.025$ p.p.m., and $0.005 < \Delta\delta_{HN} < 0.015$ p.p.m.. (C) The affected residues, in a 1 : 2 ratio, were mapped onto LAz surface according to the color code $\Delta\delta_{HN} \geq 0.025$ p.p.m., in red; $0.015 < \Delta\delta_{HN} < 0.025$ p.p.m., in blue; and $0.005 < \Delta\delta_{HN} < 0.015$ p.p.m., in grey. The four LAz proline residues were colored in black. In Panel (D) the residues with larger shifts are distributed along a loop region and a β-strand (β5), highlighted in green in the LAz backbone structure. The surface in Panel C, and respective structure in Panel D, are represented from a 'side view' of LAz β-barrel with the copper center (orange sphere) on the top, and a 'top view' facing the copper atom, on the bottom. In Panel (A) and (B) the chemical shift variation was determined using Eqn (2). Residues 1, 6, 21, and the 4 prolines, not observed in the ^1H–^{15}N HSQC spectra of LAz, are marked by an asterisk.

'cavity' behind the loop. Therefore, this loop might have some liberty to move and addition of *Ng*BCCP to the solution may cause significant perturbations in its environment. This might be an indirect effect of the formation of LAz/*Ng*BCCP ET complex and thus these residues might not be directly involved in the complex interface (*vide infra*).

The surface of both proteins was analyzed in terms of electrostatic potential and hydrophobicity to explain the nature of the small chemical shifts (grey surface). The residues located in hydrophobic patches on LAz surface experienced smaller shifts (Fig. S3), and are located on one side of the copper site and at the N-terminal end. The hydrophobic patch, surrounding His118 that coordinates the copper atom, has been proposed to be involved in complex formation of other ET complexes, as is the case of *Alcaligenes xylosoxidans* azurin and its partner nitrite reductase [40].

In *Ng*BCCP, the surface surrounding E heme is also hydrophobic (Fig. S4), which agrees with the current view that ET complexes typically have a hydrophobic surface surrounding their redox centers to promote ET [41]. LAz has an overall negative/neutral surface, although there is a small positive patch due to three surface lysines. This protein does not present a positively charged ring of residues surrounding the hydrophobic patch at the copper site as the one observed in *P. pantotrophus* pseudoazurin [7]. This charge distribution in pseudoazurin creates a large dipole moment with the vector centered at the center of mass and leaving the protein through His81, the exposed residue that coordinates the copper atom. Analysis of the dipole moment of azurins, pseudoazurin and LAz shows that azurins have a smaller dipole vector compared to pseudoazurin (Table 1). In LAz, the dipole vector is centered at its center of mass and passes through Met122 that coordinates the copper atom. Thus, even being a smaller vector, LAz positive dipole moment can pre-orient the protein with its

copper center toward *Ng*BCCP negatively charged surface, to form the 'encounter complex'.

Molecular docking simulation

The molecular docking of LAz to *Ng*BCCP was performed using two different algorithms, ZDOCK [30,42], a rigid-body docking, and BiGGER [29], a 'soft' docking, to obtain a structural model for LAz/*Ng*BCCP productive ET complex. Using ZDOCK server, the top 500 models locate LAz mainly around *Ng*BCCP E heme domain and a few solutions at the dimer interface (Fig. 4). The rdistance between LAz copper and E heme iron is shorter than 20 Å (maximum distance that enables ET [43]) in 71 of the top 100 models.

A soft-docking was performed using BiGGER and 5000 models were selected and analyzed according to the global rank and to individual ranks (geometry, electrostatic and hydrophobic scores). The top 500 solutions for global score (Fig. 5A) are distributed at the dimer interface, E domain or between E and P domains, as in ZDOCK. Analysis of the top 500 solutions ranked by hydrophobic score shows that 311 of these complexes have LAz copper atom near E heme (in 148 of these, Cu atom is within 20 Å of Fe E heme; Fig. 5B), while in the top 500 electrostatic solutions LAz is placed around the dimer interface. From these top hydrophobic scored solutions, the ones with the highest global score were clustered into six groups with slightly different conformations.

These results are consistent with the kinetic data presented before that pointed to a hydrophobic interaction, with the kinetic parameters being only slightly affected by ionic strength.

ZDOCK's top five models and BiGGER's top six models, representative of the six clusters, (Figs S5 and S6) were analyzed according to the geometrical and physicochemical properties of the protein–protein interface (Table 2). In all top models, the small

Table 1. Dipole moments for LAz and other type 1 copper proteins.

Organism	Protein	PDB ID	Redox state	Net charge[a]	Dipole moment (Debye)
Neisseria gonorrhoeae	LAz	2N0M	Reduced	−4	174
			Oxidized	−3	217
Pseudomonas aeruginosa	Azurin	4AZU	Reduced	−2	118
			Oxidized	−1	135
Achromobacter xylosoxidans	Azurin I	1RKR	Reduced	0	138
			Oxidized	+1	183
Paracoccus pantrotrophus	Pseudoazurin	3ERX	Reduced	−4	918
			Oxidized	−3	970

[a] Net charge determined for the structure with a copper atom with +1 or +2 oxidation states, respectively.
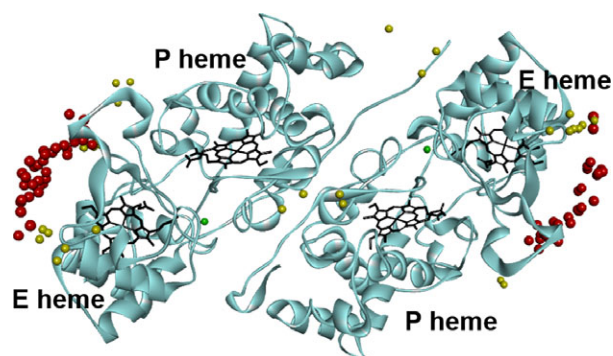
Fig. 4. Docking of LAz in *Ng*BCCP dimer using ZDOCK algorithm. The top 100 solutions are represented by LAz's copper atom position (yellow/red spheres). The copper atoms within 20 Å from the E heme iron atom are colored in red.

interface contact area agrees with a highly transient complex (822–1040 Å^2) [32,44], with a gap volume index of ~ 3 Å, consistent with other transient protein–protein complexes [44–46]. An exception was BiGGER model 2, with a larger gap volume index (4.8 Å) and a higher heme edge-Cu distance, an indication of a lower complementarity between LAz and *Ng*BCCP. Moreover, in these top models, a negative solvation free energy gain ($\Delta^i G$), upon formation of the complex, points to a hydrophobic interface, which is also supported by the large proportion of apolar residues in the interface (~ 60%) and small number of salt bridges (Table 2). All models present similar interface regions that involve small helices and loop sections surrounding the copper center, as expected in a transient interaction [21]. In addition, a small number
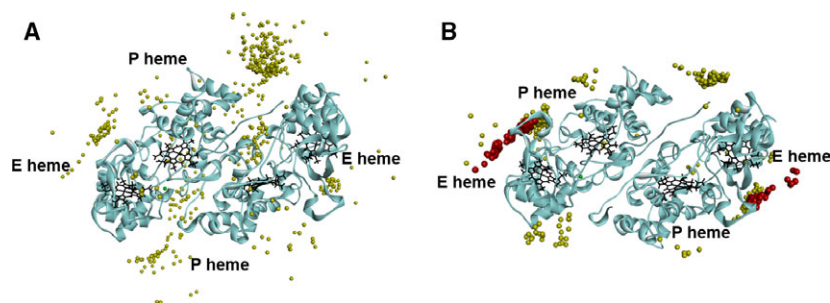

Fig. 5. Docking of LAz in *Ng*BCCP dimer using BiGGER algorithm. The top 500 solutions according to (A) global and (B) hydrophobic scores are represented by LAz's copper atom position (yellow/red spheres). In (B) the copper atoms within 20 Å from the E heme iron atom (148 solutions) are colored in red.

Table 2. Geometrical and physicochemical characteristics of the top five and six models for ZDOCK and BiGGER docking algorithms, respectively.

ZDOCK

Model	Score	Heme edge-Cu distance (Å)	ΔASA (Å^2)	Gap volume index (Å)	$\Delta^i G$ (kcal·mol^{-1})	Apolar residues (%)	H-bonds/Salt bridges
1	1112	15.5	945	2.7	−8.8	62	13/1
2	1041	10.9	864	2.5	−7.3	61	6/1
3	1032	14.7	1041	2.9	−8.6	64	4/1
4	988	9.9	784	2.9	−10.5	64	7/0
5	968	10.1	805	3.1	−11.3	60	4/0

BiGGER

Model	Global score	Hydrophobic score	Heme edge-Cu distance (Å)	ΔASA (Å^2)	Gap volume index (Å)	$\Delta^i G$ (kcal·mol^{-1})	Apolar residues (%)	H-bonds/Salt bridges
1	4.2	−4.9	16.6	994.8	3.0	−7.3	58	4/1
2	4.5	−5.1	18.4	863.2	4.8	−5.0	59	4/2
3	5.2	−7.0	18.4	924.3	3.7	−7.1	61	8/0
4	5.8	−4.8	16.5	826.8	3.1	−7.7	61	9/0
5	2.7	−7.1	15.5	877.3	3.4	−7.6	60	5/2
6	2.2	−6.0	14.3	822.5	3.3	−4.5	56	7/0

of predicted H-bonds and salt-bridges (without accounting for possible side-chain rearrangements upon complex formation), suggests that this is a weak binding [41].

There are several residues in the interface of these top model complexes that were affected in the NMR titration: Asn13, Asn15, Ala45, Val67, Gly68, Tyr74, Gly117, and His118 (Fig. 3), with Tyr74 belonging to the group of residues with the higher chemical shift variation. Mapping, onto LAz surface, the interface residues found in most of the top eleven docking complexes (Fig. 6) shows that the protein–protein interface comprises a group of residues that underwent small chemical shifts. Many of these are located at the hydrophobic patch surrounding the copper center (including His118, the surface exposed copper ligand), centered at Tyr74

(in red) and Pro116 (colored in black). Tyr74 OH group is exposed to the surface and could be involved in H-bonding upon binding. Changes in this Tyr74 would cause a series of indirect changes in the loop region, which were in fact observed in the NMR titration, due to a network of H-bonds and hydrophobic interactions between those residues that are perturbed upon *Ng*BCCP binding, such as the Val75-His85 π-alkyl interaction and the His85-Asp79 H-bond.

The LAz/*Ng*BCCP electron transfer complex

The top docking models were analyzed using PATH-WAYS to identify a potential ET pathway between the two proteins. All the best docking solutions position two LAz residues, His118 and Gly117,
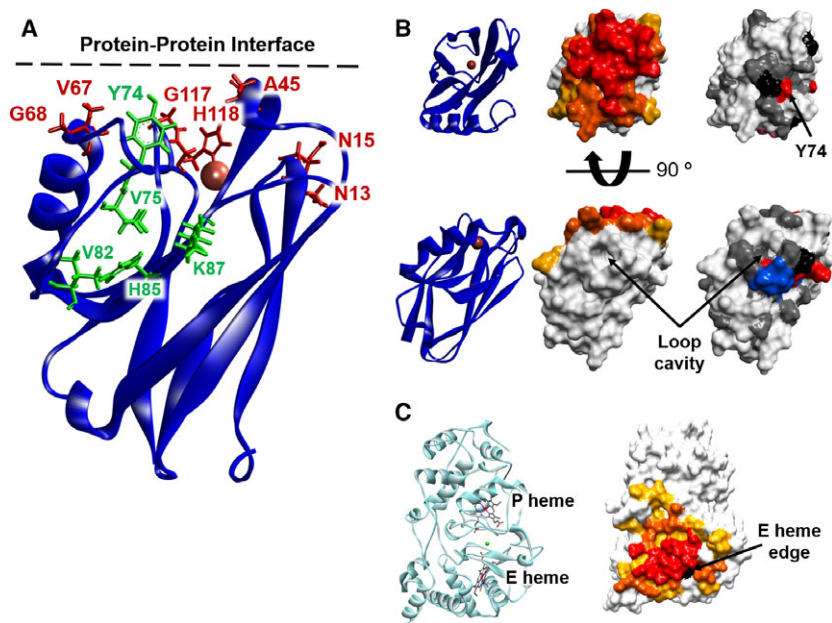

Fig. 6. Protein–protein interface surface in the docking models and comparison with the NMR data. (A) Several residues slightly shifted in the NMR spectrum (in red) are located at the proposed protein–protein interface and might be involved in H-bonds across the interface. The residues with larger chemical shifts are in the loop region (in green) and one, Tyr74, is also at the interface. The protein–protein interface surface of LAz (B) and *Ng*BCCP (C) was colored according to the frequency of the surface residue in the top eleven models previously described (> 75% models, red; 50–75% models, orange; 25–50% models, yellow). Comparison with the NMR surface map shows that the 'top side' of LAz matching the docking surface, is affected with Tyr74 close to its center, while the loop region is away from the interface surface.
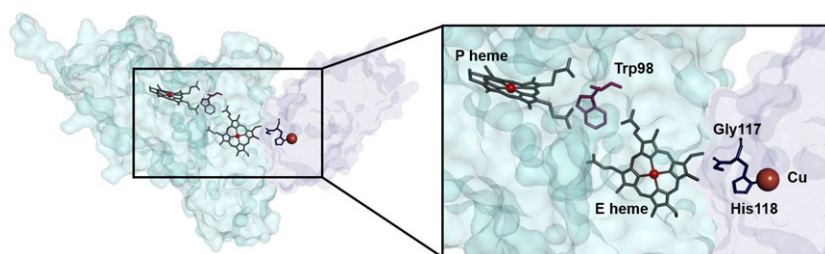

Fig. 7. Structural model of the LAz-*Ng*BCCP ET complex evidencing the ET pathway. The ET pathway starts in the copper atom, passes through His118 and then Gly117 in LAz (purple), directly to the E heme in *Ng*BCCP (blue).

near E heme. In other type 1 copper proteins, the equivalent residue of His118 (in *P. pantotrophus* pseudoazurin, His81 [6] and in *Pseudomonas aeruginosa* azurin, His117 [47]) has also been proposed to be the exit point of electrons.

The model with the highest ET rate was model 4 from ZDOCK, probably due to the shortest Heme edge-Cu distance. In this model, ET occurs between Gly117 and E heme, to its iron atom. In Fig. 7, the ET pathway from the copper site to E heme and then to P heme through the conserved Trp98 is presented.

This docking model represents one putative conformation of the LAz/*Ng*BCCP ET complex, although it is expected that there are several conformations differing between each other in the relative orientation of the two proteins and resulting in a dynamic ensemble.

The NMR data, kinetics and protein surface analysis support a model in which the formation of the LAz/*Ng*BCCP ET complex is governed by weak hydrophobic effects, directing LAz to E heme, with a positive dipole moment, which can grant the necessary pre-orientation. The small chemical shifts indicate that this ET complex has a transient nature and suggests that LAz might 'probe' different conformations, in contrast to single-orientation complexes. A similar conclusion was taken from the NMR study of bovine myoglobin and cytochrome b_5 which showed small chemical shifts that were associated to a 'dynamic ensemble of orientations' due to constant diffusion over the surface of the other protein [48].

The location of the native complex at the outer membrane might subject LAz/*Ng*BCCP ET complex to significant changes in ionic strength. Thus, the hydrophobic nature of this complex promotes high turnover numbers independently of changes in the environment, at physiological pH and temperature. Moreover, the different orientations that can be experienced by these proteins in an encounter complex *in vitro* will be restricted as both protein are membrane attached.

The work presented here contributes to the understanding of the protein interactions that occur in *N. gonorrhoeae* periplasm when this bacterium is exposed to exogenous sources of hydrogen peroxide.

Acknowledgements

Author contributions

CSN performed the experimental data presented, analyzed the data and wrote the manuscript. SRP designed and planed the project and experiments, performed the NMR experiments, contributed to the analysis and discussion of the data and wrote the manuscript.

References

1 Seib KL, Wu HJ, Kidd SP, Apicella MA, Jennings MP and McEwan AG (2006) Defenses against oxidative stress in *Neisseria gonorrhoeae*: a system tailored for a challenging environment. *Microbiol Mol Biol Rev* **70**, 344–361.

2 Pettigrew GW, Echalier A and Pauleta SR (2006) Structure and mechanism in the bacterial dihaem cytochrome c peroxidases. *J Inorg Biochem* **100**, 551–567.

3 Pettigrew GW, Prazeres S, Costa C, Palma N, Krippahl L, Moura I and Moura JJ (1999) The structure of an electron transfer complex containing a cytochrome c and a peroxidase. *J Biol Chem* **274**, 11383–11389.

4 Pettigrew GW, Pauleta SR, Goodhew CF, Cooper A, Nutley M, Jumel K, Harding SE, Costa C, Krippahl L, Moura I *et al.* (2003) Electron transfer complexes of cytochrome c peroxidase from Paracoccus denitrificans containing more than one cytochrome. *Biochemistry* **42**, 11968–11981.

5 Pettigrew GW, Goodhew CF, Cooper A, Nutley M, Jumel K and Harding SE (2003) The electron transfer complexes of cytochrome c peroxidase from Paracoccus denitrificans. *Biochemistry* **42**, 2046–2055.

6 Pauleta SR, Cooper A, Nutley M, Errington N, Harding S, Guerlesquin F, Goodhew CF, Moura I, Moura JJ and Pettigrew GW (2004) A copper protein and a cytochrome bind at the same site on bacterial cytochrome c peroxidase. *Biochemistry* **43**, 14566–14576.

7 Pauleta SR, Guerlesquin F, Goodhew CF, Devreese B, Van Beeumen J, Pereira AS, Moura I and Pettigrew GW (2004) *Paracoccus pantotrophus* pseudoazurin is an electron donor to cytochrome c peroxidase. *Biochemistry* **43**, 11214–11225.

8 Brittain T and Greenwood C (1992) Complex formation between the copper protein, azurin and the cytochrome c peroxidase of *Pseudomonas aeruginosa*. *J Inorg Biochem* **48**, 71–77.

9 Foote N, Turner R, Brittain T and Greenwood C (1992) A quantitative model for the mechanism of action of the cytochrome c peroxidase of *Pseudomonas aeruginosa*. *Biochem J* **283** (Pt 3), 839–843.

10 Ronnberg M, Araiso T, Ellfolk N and Dunford HB (1981) The reaction between reduced azurin and oxidized cytochrome c peroxidase from *Pseudomonas aeruginosa*. *J Biol Chem* **256**, 2471–2474.

11 Wu HJ, Seib KL, Edwards JL, Apicella MA, McEwan AG and Jennings MP (2005) Azurin of pathogenic *Neisseria* spp. is involved in defense against hydrogen peroxide and survival within cervical epithelial cells. *Infect Immun* **73**, 8444–8448.

12 Nóbrega CS, Saraiva IH, Carreira C, Devreese B, Matzapetakis M and Pauleta SR (2016) The solution structure of the soluble form of the lipid-modified azurin from *Neisseria gonorrhoeae*, the electron donor of cytochrome c peroxidase. *Biochim Biophys Acta* **1857**, 169–176.

13 Nóbrega CS, Raposo M, Van Driessche G, Devreese B and Pauleta SR (2017) Biochemical characterization of the bacterial peroxidase from the human pathogen *Neisseria gonorrhoeae*. *J Inorg Biochem* **171**, 108–119.

14 Woods JP, Dempsey JF, Kawula TH, Barritt DS and Cannon JG (1989) Characterization of the neisserial lipid-modified azurin bearing the H.8 epitope. *Mol Microbiol* **3**, 583–591.

15 Gotschlich EC and Seiff ME (1987) Identification and gene structure of an azurin-like protein with a lipoprotein signal peptide in *Neisseria-gonorrhoeae*. *FEMS Microbiol Lett* **43**, 253–255.

16 Li X, Parker S, Deeudom M and Moir JW (2011) Tied down: tethering redox proteins to the outer membrane in *Neisseria* and other genera. *Biochem Soc Trans* **39**, 1895–1899.

17 Turner S, Reid E, Smith H and Cole J (2003) A novel cytochrome c peroxidase from *Neisseria gonorrhoeae*: a lipoprotein from a Gram-negative bacterium. *Biochem J* **373**, 865–873.

18 Cannon JG (1989) Conserved lipoproteins of pathogenic *Neisseria* species bearing the H.8 epitope: lipid-modified azurin and H.8 outer membrane protein. *Clin Microbiol Rev* **2** (Suppl), S1–S4.

19 McLaughlin MP, Retegan M, Bill E, Payne TM, Shafaat HS, Peña S, Sudhamsu J, Ensign AA, Crane BR, Neese F *et al.* (2012) Azurin as a protein scaffold for a low-coordinate nonheme iron site with a small-molecule binding pocket. *J Am Chem Soc* **134**, 19746–19757.

20 Zaballa ME, Abriata LA, Donaire A and Vila AJ (2012) Flexibility of the metal-binding region in apo-cupredoxins. *Proc Natl Acad Sci USA* **109**, 9254–9259.

21 Acuner Ozbabacan SE, Engin HB, Gursoy A and Keskin O (2011) Transient protein-protein interactions. *Protein Eng Des Sel* **24**, 635–648.

22 Nóbrega CS, Matzapetakis M and Pauleta SR (2012) ^{1}H, ^{13}C and ^{15}N resonance assignment of the soluble form of the lipid-modified Azurin from *Neisseria gonorrhoeae*. *Biomol NMR Assign* **7**, 311–314.

23 Alberty RA and Bloomfield V (1963) Multiple intermedates in steady state enzyme kinetics. V. effect of pH on the rate of a simple enzymatic reaction. *J Biol Chem* **238**, 2804–2810.

24 Garrett DS, Seok YJ, Peterkofsky A, Clore GM and Gronenborn AM (1997) Identification by NMR of the binding surface for the histidine-containing phosphocarrier protein HPr on the N-terminal domain of enzyme I of the *Escherichia coli* phosphotransferase system. *Biochemistry* **36**, 4393–4398.

25 Pettersen EF, Goddard TD, Huang CC, Couch GS, Greenblatt DM, Meng EC and Ferrin TE (2004). UCSF Chimera-a visualization system for exploratory research and analysis. *J Comput Chem* **25**, 1605–1612.

26 Baker NA, Sept D, Joseph S, Holst MJ and McCammon JA (2001) Electrostatics of nanosystems: application to microtubules and the ribosome. *Proc Natl Acad Sci USA* **98**, 10037–10041.

27 Lotan I and Head-Gordon T (2006) An analytical electrostatic model for salt screened interactions between multiple proteins. *J Chem Theory Comput* **2**, 541–555.

28 Dolinsky TJ, Nielsen JE, McCammon JA and Baker NA (2004) PDB2PQR: an automated pipeline for the setup of Poisson-Boltzmann electrostatics calculations. *Nucleic Acids Res* **32**(Web Server issue), W665–W667.

29 Palma PN, Krippahl L, Wampler JE and Moura JJ (2000) BiGGER: a new (soft) docking algorithm for predicting protein interactions. *Proteins* **39**, 372–384.

30 Pierce BG, Wiehe K, Hwang H, Kim BH, Vreven T and Weng Z (2014) ZDOCK server: interactive docking prediction of protein-protein complexes and symmetric multimers. *Bioinformatics* **30**, 1771–1773.

31 Mintseris J, Pierce B, Wiehe K, Anderson R, Chen R and Weng Z (2007) Integrating statistical pair potentials into protein complex prediction. *Proteins* **69**, 511–520.

32 Jones S and Thornton JM (1996) Principles of protein-protein interactions. *Proc Natl Acad Sci USA* **93**, 13–20.

33 Krissinel E and Henrick K (2007) Inference of macromolecular assemblies from crystalline state. *J Mol Biol* **372**, 774–797.

34 Saha RP, Bahadur RP, Pal A, Mandal S and Chakrabarti P (2006) ProFace: a server for the analysis of the physicochemical features of protein-protein interfaces. *BMC Struct Biol* **6**, 11.

35 Regan JJ, Risser SM, Beratan DN and Onuchic JN (1993) Protein electron transport: single versus multiple pathways. *J Phys Chem* **97**, 13083–13088.

36 Betts JN, Beratan DN and Onuchic JN (1992) Mapping electron tunneling pathways: an algorithm that finds the 'minimum length'/maximum coupling pathway between

electron donors and acceptors in proteins. *J Am Chem Soc* **114**, 4043–4046.

37 Hu W, De Smet L, Van Driessche G, Bartsch RG, Meyer TE, Cusanovich MA and Van Beeumen J (1998) Characterization of cytochrome c-556 from the purple phototrophic bacterium *Rhodobacter capsulatus* as a cytochrome-c peroxidase. *Eur J Biochem* **258**, 29–36.

38 Watkins JA, Cusanovich MA, Meyer TE and Tollin G (1994) A "parallel plate" electrostatic model for bimolecular rate constants applied to electron transfer proteins. *Protein Sci* **3**, 2104–2114.

39 Rodier F, Bahadur RP, Chakrabarti P and Janin J (2005) Hydration of protein-protein interfaces. *Proteins* **60**, 36–45.

40 Paraskevopoulos K, Sundararajan M, Surendran R, Hough MA, Eady RR, Hillier IH and Hasnain SS (2006) Active site structures and the redox properties of blue copper proteins: atomic resolution structure of azurin II and electronic structure calculations of azurin, plastocyanin and stellacyanin. *Dalton Trans*, 3067–3076.

41 Crowley PB and Carrondo MA (2004) The architecture of the binding site in redox protein complexes: implications for fast dissociation. *Proteins* **55**, 603–612.

42 Pierce BG, Hourai Y and Weng Z (2011) Accelerating protein docking in ZDOCK using an advanced 3D convolution library. *PLoS ONE* **6**, e24657.

43 Winkler JR (2000) Electron tunneling pathways in proteins. *Curr Opin Chem Biol* **4**, 192–198.

44 Lo Conte L, Chothia C & Janin J (1999) The atomic structure of protein-protein recognition sites. *J Mol Biol* **285**, 2177–2198.

45 Dell'acqua S, Pauleta SR, Monzani E, Pereira AS, Casella L, Moura JJ and Moura I (2008) Electron transfer complex between nitrous oxide reductase and cytochrome c552 from Pseudomonas nautica: kinetic, nuclear magnetic resonance, and docking studies. *Biochemistry* **47**, 10852–10862.

46 Nooren IM and Thornton JM (2003) Structural characterisation and functional significance of transient protein-protein interactions. *J Mol Biol* **325**, 991–1018.

47 Gorren AC, den Blaauwen T, Canters GW, Hopper DJ and Duine JA (1996) The role of His117 in the redox reactions of azurin from *Pseudomonas aeruginosa*. *FEBS Lett* **381**, 140–142.

48 Worrall JA, Liu Y, Crowley PB, Nocek JM, Hoffman BM and Ubbink M (2002) Myoglobin and cytochrome b5: a nuclear magnetic resonance study of a highly dynamic protein complex. *Biochemistry* **41**, 11721–11730.

Supporting information

Additional Supporting Information may be found online in the supporting information tab for this article:

Fig. S1. *Ng*BCCP activation by incubation with fully reduced LAz for different time intervals.

Fig. S2. The kinetic traces of *Ng*BCCP activity with 10 μM LAz and 100 μM H_2O_2 in 10 mM MES pH 6.0. LAz oxidation was followed at A625nm in the presence (black circles) and absence (grey circles) of 2 mM CaCl2 in the assay.

Fig. S3. Analysis of LAz surface by electrostatic potential and hydrophobicity.

Fig. S4. Electrostatic and hydrophobic surface of *Ng*BCCP dimer (A) and monomer in the mixed-valence state (B,C).

Fig. S5. The five docking solutions with highest score obtained by ZDOCK.

Fig. S6. The six docking solutions using BiGGER algorithm, representing clusters of high global and hydrophobic scores.